Structural and thermodynamic properties of hexagonal BeO at high pressures and temperatures

2007 J. Phys.: Condens. Matter 19 456209

(http://iopscience.iop.org/0953-8984/19/45/456209)

IOP PUBLISHING JOURNAL OF PHYSICS: CONDENSED MATTER

J. Phys.: Condens. Matter **19** (2007) 456209 (10pp) doi:10.1088/0953-8984/19/45/456209

Structural and thermodynamic properties of hexagonal BeO at high pressures and temperatures

Hai-Feng Song[1], **Hai-Feng Liu**[1] **and Enke Tian**[2,3]

[1] Institute of Applied Physics and Computational Mathematics, Beijing 100088, People's Republic of China
[2] School of Materials Science and Technology, China University of Geosciences, Beijing 100083, People's Republic of China
[3] International Centre for Materials Physics, Chinese Academy of Sciences, Shenyang 110016, People's Republic of China

Received 15 August 2007, in final form 11 September 2007
Published 11 October 2007
Online at stacks.iop.org/JPhysCM/19/456209

Abstract

We present a first-principles scheme to study the structural and thermodynamic properties of hexagonal BeO at high pressures and temperatures, based on our recently developed modified mean-field potential (MMFP) approach. By taking the effect of the structural parameters on the free energy into account, we investigate the ground-state properties of BeO at ambient conditions, structural parameters varying with temperature and pressure, thermal equation of state, and Hugoniot curve. The calculated properties are in good agreement with available experimental data and other theoretical results.

(Some figures in this article are in colour only in the electronic version)

1. Introduction

The properties of insulating refractory oxides at high pressures and high temperatures are important in both ceramics and materials science. BeO is of particular importance because of its high-thermal conductivity and low-electrical conductivity [1]. As a member of the series of alkaline-earth oxides, BeO is the only one to crystallize in the hexagonal wurtzite rather than in the rock-salt structure. Further, not only is BeO harder than the other alkaline-earth oxides but also it is among the hardest materials known. These interesting physical properties are related to characteristic features of interatomic bonding in BeO [2].

The main driving force for the previous theoretical studies of BeO was to investigate pressure-induced phase transformation [3–7], which was motivated by the well known dielectric theory about the structural phase stabilities of A^NB^{8-N} compounds [8]. A significant discrepancy exists in the phase transition sequence and the magnitude of the transition pressure. On the other hand, a few theoretical calculations were performed to investigate the elastic properties of BeO [9–11].

It is worth noting that the theoretical calculations mentioned above only gave material properties at zero temperature, without any thermal effects included. Therefore, it is necessary to examine the thermal influences on the properties of BeO. To address this interest, in this paper, we concentrate on the structural and thermodynamic properties of hexagonal BeO at high pressures and temperatures, by using first-principle calculations combined with our newly developed modified mean-field potential (MMFP) approach.

Zero-temperature properties of materials can be obtained in a straightforward way using first-principles electronic structure methods, but thermal properties are much more difficult to obtain from first principles. Four approaches have been used: application of the phenomenological Debye model [12, 13], quasiharmonic lattice dynamics [14, 15], molecular dynamics [16, 17], and the particle-in-a-cell (PIC) method [18–20]. Each approach has its advantages and disadvantages: the Debye model is quick and easy, but usually works out anharmonic contributions; quasiharmonic lattice dynamics is very computationally intensive and neglects anharmonicity at a constant volume; molecular dynamics is even more computationally intensive, usually requiring small system sizes and neglecting quantum occupation of phonon states; and PIC requires supercells and neglects correlations between atomic motions, but it includes anharmonic terms which are important at high temperatures.

Because the PIC calculation is also very time consuming and inconvenient, we develop a MMFP approach based on the works of Wang *et al* [21–23]. We have shown that our MMFP approach correctly describes most of the structural and thermodynamic properties of low-symmetry metal [24]. MMFP is also probably the fastest of the more accurate approaches for thermal properties of complex systems with the quasimonatomic crystal types, such as NaCl and BeO. Here we test the accuracy by comparing our calculated properties of hexagonal BeO at high pressures and high temperatures with the experimental data and other theoretical results.

The rest of this paper is organized as follows. In section 2, we present the general theory of the MMFP approach. In section 3, we present our calculated structural and thermodynamic properties of hexagonal BeO, and compare those with the experimental data and other theoretical results. The results are encouraging. Finally, our summary is given in section 4.

2. Computational methods

The MMFP approach is based on the mean-field potential (MFP) model [21–23], and expends it to more general cases where the effect of the structural parameters varying with volume on the total free energy is taken into account, so that the MMFP approach can be presented for low-symmetry or complex structure crystals. For a crystal with a given temperature T and a given cell volume V that is a function of the structural parameters $\{a_i\}$, the Helmholtz free energy $F[V(\{a_i\}), T]$ per cell can be written as

$$F[V(\{a_i\}), T] = E_c[V(\{a_i\})] + F_{\rm el}[V(\{a_i\}), T] + F_{\rm ion}[V(\{a_i\}), T], \qquad (1)$$

where $E_c[V(\{a_i\})]$ is the zero-temperature energy, i.e. the ground-state energy when the ions are fixed at their lattice sites, $F_{\rm el}[V(\{a_i\}), T]$ is the thermal free energy from electronic excitations, and $F_{\rm ion}[V(\{a_i\}), T]$ is the vibrational contribution to the free energy.

The zero-temperature energy $E_c[V(\{a_i\})]$ can be calculated using density functional theory [25, 26] within the generalized-gradient approximation. The electronic contribution $F_{\rm el}[V(\{a_i\}), T]$ and the vibrational contribution $F_{\rm ion}[V(\{a_i\}), T]$ to the free energy can be obtained as implemented in [24].

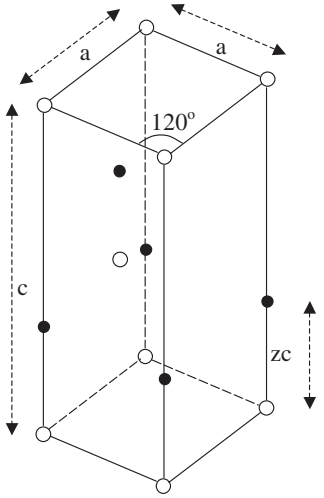

Figure 1. The unit cell of BeO in the hexagonal wurtzite structure. There are two atoms of each kind in the unit cell on the special positions: beryllium atoms at (0, 0, 0) and $(1/3, 2/3, 1/2)$ and oxygen atoms at $(0, 0, z)$ and $(1/3, 2/3, 1/2 + z)$. Open spheres denote cations and black spheres are anions.

The equilibrium structure of the crystal at any T and V can be determined by minimizing the Helmholtz free energy

$$F[V(\{a_i\}), T] = E_c[V(\{a_i\})] + F_{\text{el}}[V(\{a_i\}), T] + F_{\text{ion}}[V(\{a_i\}), T], \tag{2}$$

with respect to all the structural parameters $\{a_i\}$. Once knowing the minimal Helmholtz free energy $F(V, T)$ at a given T and V, namely, the free energy corresponding to the equilibrium structure at a given T and V, other thermodynamic functions and the thermal properties of the crystal can be deduced. For example, internal energy $E(V, T)$, pressure $P(V, T)$, and the isothermal bulk modulus $B_T(V, T)$ can be respectively calculated by

$$E(V, T) = F(V, T) - T\left(\frac{\partial F(V, T)}{\partial T}\right)_V, \tag{3}$$

$$P(V, T) = -\left(\frac{\partial F(V, T)}{\partial V}\right)_T, \tag{4}$$

$$B_T(V, T) = V\left(\frac{\partial^2 F(V, T)}{\partial V^2}\right)_T. \tag{5}$$

3. Results and discussion

BeO crystallizes in the hexagonal wurtzite structure with the space group $P6_3mc$. There are two atoms of each kind in the unit cell on the special positions as shown in figure 1: beryllium atoms at (0, 0, 0) and $(1/3, 2/3, 1/2)$ and oxygen atoms at $(0, 0, z)$ and $(1/3, 2/3, 1/2+z)$. The structure is thus defined by two lattice constants, a and c, and the internal structural parameter, z. In fact, at a given V and T, for the determination of Helmholtz free energy of the hexagonal wurtzite structure, it is enough to minimize the function $F[V(\{a_i\}), T] = F(V, c/a, z, T)$ with respect to two variables, namely, the c/a ratio and z.

The zero-temperature energy calculations are performed using the Vienna *ab initio* simulation package [27, 28], which is based on the density functional theory. Exchange and correlation functional is given by the generalized-gradient approximation of Perdew–Burke–Ernzerhof (PBE) form [29]. Electron–ion interaction is represented by the projector-augmented wave (PAW) method [30] as implemented by Kresse and Joubert [31]. The PAW method is an all-electron technique similar to other standard implementations such as full-potential

Table 1. Calculated and experimental structural parameters, the isothermal bulk modulus, and its pressure derivative for hexagonal BeO under ambient pressure.

	a (Å)	c (Å)	c/a	z	B_0 (GPa)	B_0'
LDA (0 K)[a]	2.667	4.355	1.633		239	
GGA (0 K)[b]	2.703	4.379	1.620	0.377	203	
GGA (0 K)[c]	2.741	4.457	1.626	0.377		
GGA (0 K)[d]	2.701	4.387	1.624	0.3777	206	3.33
GGA (0 K)[e]	2.712	4.404	1.624	0.3778	209	3.48
GGA (298 K)[f]	2.719	4.417	1.624	0.3778	204	3.59
Experiment (298 K)[g]	2.696	4.379	1.624	0.3781	210	5.1

[a] From [5], all-electron (FPLMTO) LDA calculations.
[b] From [6], GGA + soft nonlocal pseudopotential.
[c] From [7], GGA + ultrasoft pseudopotential.
[d] From [11], GGA + ultrasoft pseudopotential.
[e] This work, all-electron (PAW) GGA calculations.
[f] This work, all-electron (PAW) GGA calculations.
[g] From [35].

linear-augmented plane waves (FLAPW) [32]. as well as being closely related to the ultrasoft pseudopotential (USPP) method [33]. We test kinetic energy cutoff and k-point sampling to assure a total energy convergence of 15 meV per cell including four atoms. As a result of the convergence tests, the kinetic energy cutoff is 520 eV for all calculations, and the k-point meshes of Brillouin zone sampling based on the Monkhorst–Pack scheme [34] are $15 \times 15 \times 15$.

3.1. Ground-state properties

As mentioned above, we evaluate the Helmholtz free energies at different volumes and temperatures by a direct minimization over the c/a ratio and z of the free energy $F(V, c/a, z, T)$. From the resulting free energies, we calculate the ground-state properties of hexagonal BeO under ambient conditions and summarize them in table 1. It is found that the equilibrium lattice constants and bulk modulus, in special the c/a ratio and the internal structural parameter z, are in good agreement with the experimental values [35].

In table 1, we also calculate zero-temperature properties of BeO under ambient pressure, which are in better agreement with the other theoretical GGA results [6, 7, 11] than the LDA result [5]. On the other hand, from our calculated results of room-temperature and zero-temperature, it is shown that the contribution of thermal expansivity results in a 0.3% increase in both lattice parameters, and causes the isothermal bulk modulus to decrease by 2%.

3.2. Structural changes at high pressures and temperatures

Figure 2 displays the structural parameters of hexagonal BeO as a function of pressure at room temperature. From figure 2, it is clearly shown that the calculated relative lattice constants, the c/a ratio, and the internal structural parameter z are in excellent agreement with the experimental data [35]. At room temperature, the lattice constants decrease continuously with increasing pressure, and the a axis is more compressible than the c axis. The linear compressibilities calculated from linear fits to the $a(P)$ and $c(P)$ dependencies of 0–5 GPa are almost identical for the two axes: $\beta_a = 1.52$ TPa^{-1} and $\beta_c = 1.50$ TPa^{-1}. These results agree well with the experimental low-pressure data of 1.50 ± 0.04 and 1.46 ± 0.03 TPa^{-1}, respectively [35]. We further evaluate the linear compressibilities from

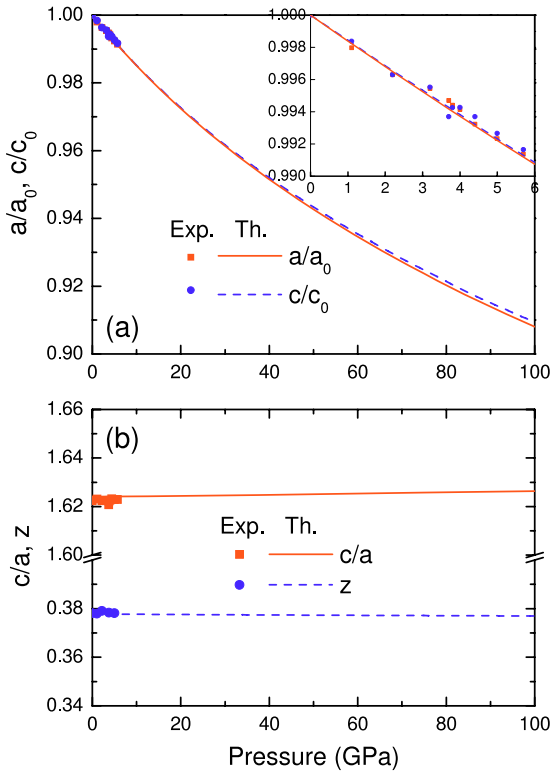

Figure 2. Calculated structural parameters of hexagonal BeO as a function of pressure at room temperature compared with experimental data from [35]: (a) the relative lattice constants L/L_0 ($L = a, c$), and (b) the c/a ratio and the internal structural parameter z. L_0 ($L = a, c$) is the lattice constant of BeO under ambient conditions.

higher-order polynomial fitting of the $a(P)$ and $c(P)$ data, using a function of the form

$$L(P)/L_0 = 1 + \beta_L P + \sum_{n=2} k_n P^n \qquad (L = a, c). \tag{6}$$

This procedure is applied to the data in the range between 0 and 100 GPa, and gives $\beta_a = 1.61$ TPa^{-1} and $\beta_c = 1.58$ TPa^{-1}. The results agree with the other theoretical results [11] of 1.63 and 1.62 TPa^{-1}, and are statistically more reliable than the low-pressure linear fitting ones.

As shown in figure 2(b), the c/a ratio displays a slight increase from 1.624 at ambient pressure to only 1.626 at 100 GPa. Further analysis shows that the c/a ratio at pressures below 5 GPa is practically unchanged with $\mathrm{d}(c/a)/\mathrm{d}P = 0.001$ TPa^{-1}. This result is smaller than that of Milman *et al* with 0.05 TPa^{-1} [11], more consistent with the experimental conclusion that the c/a ratio did not vary with pressure [35]. Semiempirical results obtained using the potential-induced breathing (PIB) model give quite a different value for the pressure derivative of the c/a ratio, -0.29 TPa^{-1} [9]. This indicates that our approach well reproduces the delicate pressure-induced structural changes in the BeO crystal.

The internal parameter z, the only other structural parameter that might be responsible for structural changes, decreases by 0.2% over the pressure range of 100 GPa as shown in figure 2(b). At pressure between ambient pressure and 5 GPa, our calculations give

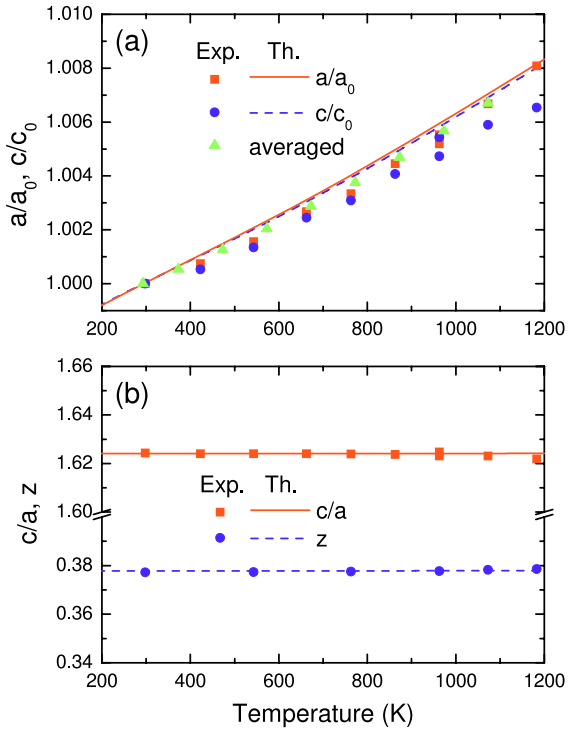

Figure 3. Calculated structural parameters of hexagonal BeO as a function of temperature at ambient pressure. (a) The solid and dashed lines correspond to the theoretical relative lattice constants which are practically identical for the two axes. Squares and circles represent experimental data from [35], and triangles represent experimental data from [36], which give averaged thermal expansion. L_0 ($L = a, c$) is the lattice constant of BeO under ambient conditions. (b) The solid and dashed lines correspond to the theoretical c/a ratio and the internal structural parameter z, respectively, and squares and circles represent experimental data from [35].

$\mathrm{d}z/\mathrm{d}P = -0.01$ TPa^{-1}, which is compatible with the experimental conclusion that z did not vary significantly with pressure [35] and other theoretical results [11].

Figure 3 displays the structural parameters of hexagonal BeO as a function of temperature at ambient pressure, which are in good agreement with the available experimental data [35, 36]. As shown in figure 3(a), the calculated lattice constants increase slowly with increasing temperature, and the thermal expansion of the a axis α_a is very slightly larger than that of the c axis α_c at temperatures above 293 K, where the thermal expansion can be expressed as $\alpha_L(T) = L(T)/L_0 - 1$ ($L = a, c$). The experiment [36] gave the averaged thermal expansion without showing the difference of α_a and α_c, while the experiment [35] showed that α_a was slightly larger than α_c. From figure 3(a), it can be seen that our calculated results are in better agreement with the experiment [36] than those of Hazen *et al* [35]. We also calculate the average volume thermal expansion coefficient of BeO between room temperature and 1200 K, 2.77×10^{-5} K^{-1}, which is very close to the experimental data of $2.66 \pm 0.10 \times 10^{-5}$ K^{-1} [35].

Further analysis of the experiment [35] indicates that below 900 K the difference between the expansions of the a and c axes is very small and less than 0.04%, and above 900 K the difference becomes slightly larger and arrives at 0.15% at 1183 K; while our calculation shows the difference is less than 0.02%. The discrepancy between the experiment [35] and our calculation may be caused by the follows. First, the crystal in the theoretical calculation

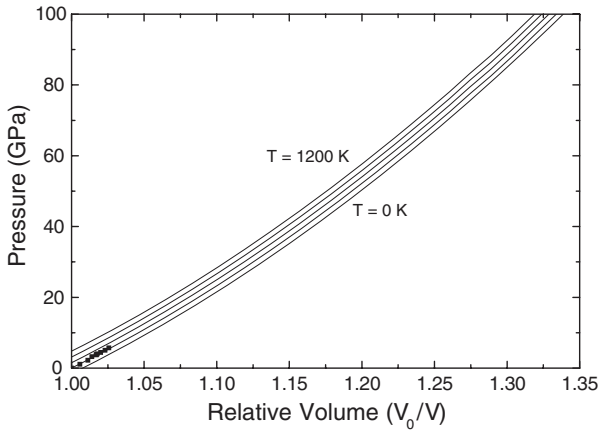

Figure 4. Theoretical thermal equation of state at different temperatures. The curves (from bottom to top) correspond to temperatures from 0 to 1200 K with 300 K interval, and squares represent room-temperature experimental data [35]. V_0 is the unit-cell volume under ambient conditions.

is pure and ideal BeO, while the sample in the experiment is synthetic BeO, bromellite, which includes other components such as Al_2O_3, SiO_2, and H_2O. These components seem a likely cause of the observed behavior in the thermal expansions of the *a* and *c* axes. On the other hand, our approach might neglect some effects which have contributed to the thermal expansions of the two axes. These possibilities can perhaps best be resolved by first-principles molecular dynamics simulations with a large number of atoms at high temperatures.

From figure 3(b), it can be seen that the c/a ratio shows an excellent agreement with the experimental data [35]: at temperature below 900 K the theoretical and experimental c/a ratios are practically equal, and at temperatures between 900 and 1200 K the theoretical c/a ratio is only 0.06% smaller than the experimental results.

The internal parameter z undergoes a small increase with temperature as shown in figure 3(b). Between room temperature and 1200 K, the calculated z parameter increases from 0.3778 to 0.3779 Å. Hazen *et al* [35] observed a similar increase from 0.3771 ± 0.0020 to 0.3785 ± 0.0020 Å by using x-ray diffraction, and Pryor *et al* [37] observed an increase from 0.3778 ± 0.0010 to 0.3795 ± 0.0010 Å in their high-temperature neutron-diffraction study.

3.3. Thermodynamic properties at high pressures and temperatures

In figure 4 we plot the thermal equation of state of hexagonal BeO at temperatures between 0 and 1200 K. The calculated thermal equation of state at 300 K exactly goes through experimental measurements at room temperature [35]. From figure 4, it is also clearly shown that because of the thermal pressure contribution from the electron excitations and lattice vibrations, the total pressure at the same volume increases with increasing temperature.

The thermal pressure can be obtained from the pressure difference between isotherms, namely, $P_{\rm th}(V, T) = P(V, T) - P(V, T = 0)$. The thermal pressures as a function of relative volume V_0/V are shown in figure 5(a). At low temperature, the thermal pressures are small, and show little volume dependence. At elevated temperature, the magnitudes of the thermal pressures increase significantly, and their values first show a small decrease with increase of relative volume, and then show an increase. The thermal pressures as a function of temperature are shown in figure 5(b). At a given volume, the thermal pressure shows a nearly linear increase

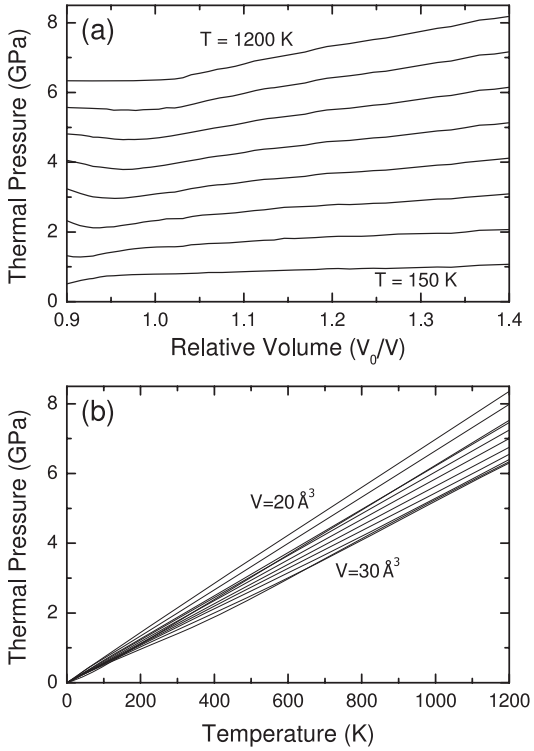

Figure 5. Thermal pressure of hexagonal BeO (a) as a function of relative volume for temperatures from 150 up to 1200 K with 150 K interval, and (b) as a function of temperature for volumes varying from 20 to 30 Å^3/cell with 10 Å^3/cell interval. V_0 is the unit-cell volume under ambient conditions.

with temperature. Moreover, the thermal pressures show a strong volume dependence. This is different from bcc Ta, where the thermal pressure has a slope of ∼0.004 42 GPa K^{-1} for almost all the volumes [19]. The different thermal pressure behavior of BeO might be partly due to the effect of the structural parameters varying with volume, which is similar to the case of hcp Be [24].

Besides experimental data obtained under hydrostatic pressure using a diamond anvil cell [35, 38], the source of information on the equation of state of BeO at high compression and high temperatures is shock-wave data [39]. From shock-wave data, which are characterized by shock velocity D and particle velocity u, one can define Hugoniot states with $V_H/V_0 = (D - u)/D$ and $P_H = \rho_0 Du$, where P_H and V_H are the final pressure and volume, and V_0 and ρ_0 are the initial volume and density. To compare our results of the equation of state of BeO at high compression and high temperatures with those derived from the shock-wave data, we calculated the pressures P_H and temperatures T_H on the Hugoniot of BeO by solving the Rankine–Hugoniot equation

$$P_H(V_0 - V_H) = 2(E_H - E_0), \tag{7}$$

where E_H is the internal energy along the Hugoniot, and E_0 is the initial internal energy corresponding to the experimental initial volume V_0. In order to reproduce the experimental initial volume [39], we subtract 4.32 GPa from each pressure and modify the energies in a consistent fashion, as was done in [5]. For a given volume V, the temperature T_H on

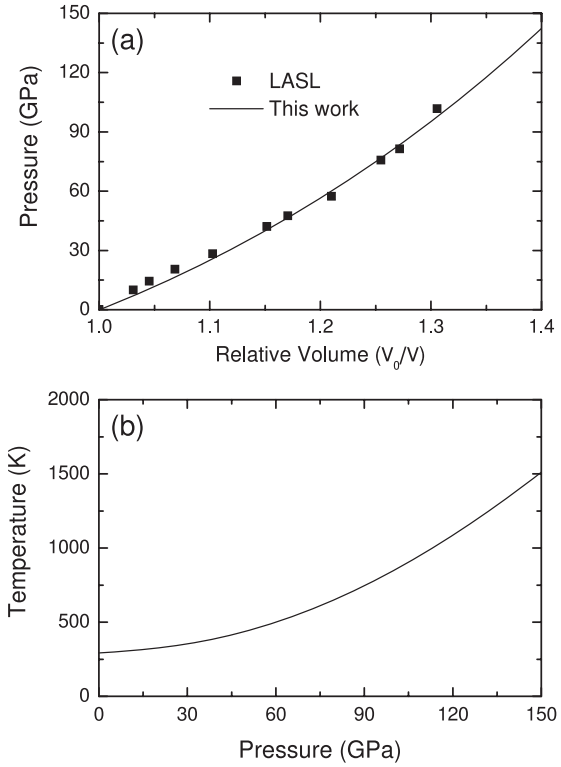

Figure 6. (a) Theoretical Hugoniot for hexagonal BeO (solid line) compared with experimental Hugoniot data (squares) from [39]. (b) Theoretical temperatures along the Hugoniot.

the Hugoniot is varied until equation (7) is satisfied. The calculated Hugoniot for BeO is plotted in figure 6 and compared with the experimental data [39]. It is worth noting that the experimental data included large strength effects that increased the measured shock velocity and stress relative to the theoretical Hugoniot, and these effects would be most noticeable for small u and would diminish as u was increased. In this regard, the overall agreement between our calculation and the experiment is very good up to the experimentally attainable Hugoniot pressure of 102 GPa, except for four points in the range between 0 and 30 GPa where the strength effects are large. In this paper, we do not consider the effect of phase transition on the Hugoniot. Because the scheme we have presented here depends on the crystal structures and permits efficient computation, we hope to be able to present a detailed discussion about the phase transition and the corresponding multiphase equation of state for BeO in a later work.

4. Conclusions

In this paper, based on our newly developed MMFP approach, we present a first-principles scheme to study the structural and thermodynamic properties of hexagonal BeO at high pressures and temperatures. Because BeO has a complex structure with the hexagonal wurtzite crystal type, we consider the effect of the structural parameters varying with volume on the total free energy. We investigate the ground-state properties at ambient conditions, structural parameters varying with temperature and pressure, thermal equation of state, and Hugoniot curve, which show a good agreement with available experimental data and other theoretical

results. These demonstrate that our scheme also correctly describes most of the structural and thermodynamic properties of complex structure systems, in addition to low-symmetry metals [24].

Acknowledgments

This work is supported by the National Natural Science Foundation of China (Grants Nos 10135010 and 10575015) and the Science Foundation of China Academy of Engineering Physics, China (Grant No. 2002Z01041).

References

[1] Vidal-Valat G, Vidal J P, Kurki-Suonio K and Kurki-Suonio R 1987 *Acta Crystallogr.* A **43** 540
[2] Joshi K B, Jain R, Pandya R K, Ahuja B L and Sharma B K 1999 *J. Chem. Phys.* **111** 163
[3] Chang K J, Froyen S and Cohen M L 1983 *J. Phys. C: Solid State Phys.* **16** 3475
[4] Van Camp P E and Van Doren V E 1996 *J. Phys.: Condens. Matter* **8** 3385
[5] Boettger J C and Wills J M 1996 *Phys. Rev.* B **54** 8965
[6] Park C J, Lee S G, Ko Y J and Chang K J 1999 *Phys. Rev.* B **59** 13501
[7] Cai Y, Wu S, Xu R and Yu J 2006 *Phys. Rev.* B **73** 184104
[8] Phillips J C 1970 *Rev. Mod. Phys.* **42** 317
[9] Jephcoat A P, Hemley R J, Mao H K, Cohen R E and Mehl M J 1988 *Phys. Rev.* B **37** 4727
[10] Lichanot A and Rerat M 1993 *Chem. Phys. Lett.* **211** 249
[11] Milman V and Warren M C 2001 *J. Phys.: Condens. Matter* **13** 241
[12] Moruzzi V L, Janak J F N and Schwarz K 1988 *Phys. Rev.* B **37** 790
[13] Sinko G V and Smirnov N A 2002 *J. Phys.: Condens. Matter* **14** 6989
[14] Sha X and Cohen R E 2006 *Phys. Rev.* B **73** 104303
[15] Karki B B, Wentzcovitch R M, de Gironcoli S and Baroni S 2000 *Phys. Rev.* B **61** 8793
[16] Oganov A R, Brodholt J P and Price G D 2001 *Nature* **411** 934
[17] Oganov A R, Brodholt J P and Price G D 2000 *Phys. Earth Planet. Inter.* **122** 277
[18] Wasserman E, Stixrude L and Cohen R E 1996 *Phys. Rev.* B **53** 8296
[19] Cohen R E and Güseren O 2001 *Phys. Rev.* B **63** 224101
[20] Xiang S, Cai L C, Bi Y, Jing F and Wang S 2005 *Phys. Rev.* B **72** 184102
[21] Wang Y 2000 *Phys. Rev.* B **61** R11863
[22] Wang Y, Chen D and Zhang X 2000 *Phys. Rev. Lett.* **84** 3220
[23] Wang Y, Liu Z K, Chen L Q, Burakovsky L, Preston D L, Luo W, Johansson B and Ahuja R 2005 *Phys. Rev.* B **71** 054110
[24] Song H F and Liu H F 2007 *Phys. Rev.* B **75** 245126
[25] Hohenberg P and Kohn W 1964 *Phys. Rev.* **136** B864
[26] Kohn W and Sham L J 1965 *Phys. Rev.* **140** A1133
[27] Kresse G and Hafner J 1993 *Phys. Rev.* B **48** 13115
[28] Kresse G and Furthmüller J 1996 *Phys. Rev.* B **54** 11169
Kresse G and Furthmüller J 1996 *Comput. Mater. Sci.* **6** 15
[29] Perdew J P, Burke K and Ernzerhof M 1996 *Phys. Rev. Lett.* **77** 3865
[30] Blöchl P E 1994 *Phys. Rev.* B **50** 17953
[31] Kresse G and Joubert D 1999 *Phys. Rev.* B **59** 1758
[32] Wei S H and Krakauer H 1985 *Phys. Rev. Lett.* **55** 1200
[33] Vanderbilt D 1990 *Phys. Rev.* B **41** 7892
[34] Monkhorst H J and Pack J D 1976 *Phys. Rev.* B **13** 5188
[35] Hazen R M and Finger L W 1986 *J. Appl. Phys.* **59** 3728
[36] Kirby R K, Hahn T A and Rothrock B D 1972 *American Institute of Physics Handbook* 3rd edn, ed D E Gray (New York: McGraw-Hill) pp 4–119
[37] Pryor A W and Sabine T M 1964 *J. Nucl. Mater.* **14** 275
[38] Mori Y, Niiya N, Ukegawa K, Mizuno T, Takarabe K and Ruoff A L 2004 *Phys. Status Solidi* b **241** 3198
[39] Marsh S P 1980 *Los Alamos Shock Hugoniot Data* (Berkeley, CA: University of California Press)